Journal of Alloys and Compounds 643 (2015) 247–252

Contents lists available at ScienceDirect

Journal of Alloys and Compounds

journal homepage: www.elsevier.com/locate/jalcom

Theoretical spectra identification and fluorescent properties of reddish orange Sm-doped $BaTiO_3$ phosphors

Lei Zhang [a], Hong Pan [a], Honggang Liu [b,*], Binbin Zhang [a], Long Jin [a], Minhao Zhu [a], Weiqing Yang [a,*]

[a] Key Laboratory of Advanced Technologies of Materials (Ministry of Education), School of Materials Science and Engineering, Southwest Jiaotong University, Chengdu 610031, China
[b] Department of Materials Science, Sichuan University, Chengdu 610064, China

ARTICLE INFO

Article history:
Received 28 February 2015
Received in revised form 10 April 2015
Accepted 13 April 2015
Available online 25 April 2015

Keyword:
White LEDs
Fluorescent spectra
Complete diagonalization method
$BaTiO_3$: Sm^{3+}

ABSTRACT

The reddish orange Sm^{3+}-doped tetragonal perovskite $BaTiO_3$ (BTO) phosphors for white LEDs were synthesized by the simple solid state reaction method. These phosphors, which can be effectively excited by the near ultraviolet light 409 nm ($^6P_{3/2}$ (Γ_7) → $^6H_{5/2}$ (Γ_7)), produces the emitted reddish orange light peaks locate at about 561 nm, 595 nm and 643 nm originated from the transitions of $^4G_{5/2}$ (Γ_7) → $^6H_{5/2}$ (Γ_7), $^4G_{5/2}$ (Γ_7) → $^6H_{7/2}$ (Γ_7) and $^4G_{5/2}$ (Γ_7) → $^6H_{9/2}$ (Γ_7). Moreover, in order to calculate the fluorescent spectra of these phosphors, the complete 2002 × 2002 energy matrix was successfully constructed by an effective operator Hamiltonian including the free ion and crystal field interactions. Sixteen experimental fluorescent spectra in visible light range for Sm^{3+} ion at the tetragonal (C_{4v}) Ba^{2+} site of BTO crystal, firstly, were accurately and quantitatively indentified from a complete diagonalization (of energy matrix) method (CDM) through only five crystal field parameters. The fitting values are very close to the experimental results, evidently proving the capability of CDM to investigate the luminescent phosphors alike in kind for w-LEDs.

1. Introduction

Rare-earth (RE) elements doped phosphors, due to the inherent chemical and physical stability ascribed to a partially filled inner ($4f^n$) shell shielded from its surroundings by completely filled outer ($5s^2$ and $5p^6$) orbitals, reach overwhelming superiority over other phosphors in the fields of optoelectronic and photonic applications, ranging from solid-state lasers, displays to optical fiber telecommunication and phosphors for colors lamps [1–9]. Among them, trivalent samarium Sm^{3+} with $4f^5$ configuration has the excellently stable emission spectra in the range of visible light originated from the various possible transitions among ^6H, ^6P, ^4G, ^4F, ^4I, and ^4M, suggesting that Sm^{3+}-doped phosphors for the application of light emitting diodes (LEDs), especially for white LEDs [10,11,4]. However, the identifications of those spectra were often determined through the previous reports and then their mechanisms are quite unphilosophical to date.

Besides, barium titanate ($BaTiO_3$, short for BTO) is one of the important ferroelectrics with a typical perovskite structure (ABO_3). Thanks to its important applications in field of ferroelectric sensors, optoelectronic devices, actuators, and so on, a lot of reports mainly focused on the dielectric, piezoelectric and ferroelectrics effects [12–14]. Although the luminescence of $BaTiO_3$ containing Sm^{3+} has been previously investigated by Makishima et al. [15,16]. In the far past, a fixed 365 nm excitation light had been applied to investigate the emission light of as-grown crystals due to the limited test technique at that time. The best excitation wavelength was difficultly determined and then the strongest emission light was obtained. Moreover, the divalent Ba^{2+} is replaced by trivalent Sm^{3+}, which producing the charge imbalance. It is necessary that a monovalent cation like Na^+, K^+ and Li^+ acted as a charge compensator [17,18] for effectively enhancing the emission spectra intensity of as-grown phosphors. However, the related works been rarely reported to date.

Here, we reported a novel reddish orange $Ba_{1-x}TiO_3$: Sm_x (x = 0.01–0.06) (BTOS) phosphors for w-LEDs by the simple and effective solid state reaction. The doping concentrations (wt%) of Na_2CO_3, as the charge compensation of charge imbalance due to the substitute of Sm^{3+} for Ba^{2+} in the perovskite $BaTiO_3$ crystals, have been optimized in the range of 0–7 wt%. More importantly, the complete diagonalization (of energy matrix) method (CDM) of crystal field theory (CFT) was used to all-sidedly and accurately identify these spectra of Sm^{3+} ion in tetragonal crystals by the complete 2002 × 2002 energy matrix, which is established by an effective operator Hamiltonian including the free ions and crystal field interactions. The as-grown reddish orange BTOS phosphors can

* Corresponding authors. Tel.:+86 28 87600415.
E-mail addresses: liuhg@scu.edu.cn (H. Liu), wqyang@swjtu.edu.cn (W. Yang).

http://dx.doi.org/10.1016/j.jallcom.2015.04.087
0925-8388/

produce the strong emission spectra about 561 nm, 595 nm and 637 nm when effectively excited by the near ultraviolet light about 409 nm. For the first time, these main spectra were confirmed to be ascribed to the transitions of $^6P_{3/2}$ (Γ_7) → $^6H_{5/2}$ (Γ_7) (409 nm), $^4G_{5/2}$ (Γ_7) → $^6H_{5/2}$ (Γ_7) (561 nm), $^4G_{5/2}$ (Γ_7) → $^6H_{7/2}$(Γ_7) (595 nm) and $^4G_{5/2}$ → $^6H_{9/2}$(Γ_7) (637 nm). Furthermore, the transition originations of other experimental 14 spectra in the range of visible light accurately and theoretically indentified by CDM method, which would unambiguously present a deep and thorough understanding on the fluorescent mechanism of Sm^{3+} ion at the tetragonal (C_{4v}) Ba^{2+} site of $BaTiO_3$ crystal and give strong impetus to the further development of rare earth ions doped phosphors for w-LED.

2. Experimental methods

The reddish orange phosphors BTOS were prepared by the simple solid state reaction method. $BaCO_3$ (99.5%), Sm_2O_3 (99.99%) and TiO_2 (99.9%) were selected as the source materials. Na_2CO_3 (99.5%) served as both a latent solvent of crystal growth and the charge compensation of charge imbalance due to the substitute of Sm^{3+} for Ba^{2+} in the perovskite $BaTiO_3$ crystals. The concentration range of Na_2CO_3 is 0–7 wt% of all the other starting materials total quality. The corresponding stoichiometric amount of starting materials were mixed homogeneously in an agate mortar and pre-annealed at 500 °C for 3 h, then annealed at 1100 °C for 5 h.

The crystal structure properties and the unite cell volumes of the reddish orange phosphors BTOS were investigated by the X'Pert Pro MPD (Holland) X-ray diffractometer with Cu Kα_1 radiation (λ = 0.154 nm). The morphology and stoichiometric amount of the as-grown reddish orange phosphors were examined by scanning electron microscopy (SEM, S4800) and energy-dispersive X-ray spectroscopy (EDX, S4800), respectively. Their room temperature photoluminescent (PL) spectra were investigated by Hitachi F7000 spectrofluorometer using a 150 W xenon lamp as excitation energy source.

3. Results and discussion

3.1. Crystal structure and morphology characterization

All XRD patterns of the reddish phosphors BTOS were shown in Fig. 1a, in which, their XRD patterns are in good agreement with data in Inorganic Crystal Structure Database (PDF#81-2201), predicting that Sm^{3+}-doped combinations do not generate any impurity in host structure. Furthermore, as shown in Fig. 1b, the gradually decreasing of tetragonality (c/a) with the increase of Sm^{3+}-doped concentration obviously reveals the transformation from tetragonal to cubic structure [11,10]. This result provides the quite importantly experimental data for theoretical identification of fluorescent spectra of as-grown phosphors.

Usually, the size and shape of as-grown phosphors for white LEDs would affect their luminous and heat dissipation efficiency and then SEM images of reddish orange BTOS phosphors were investigated in detail. Fig. 2a and b shows the BTOS crystalline grains are with a diameter around 2–4 μm, which is in favor of the encapsulation in white LEDs. Moreover, in Fig. 2c, the nominal stoichiometry of the reddish orange phosphors $Ba_{0.98}TiO_3$: $Sm_{0.02}$ was verified by EDS. The atom number ratio N_{Ba}:N_{Ti}:N_{Sm} (9.51:9.85:0.22) is close to the stoichiometry of $Ba_{0.98}TiO_3$: $Sm_{0.02}$, indicating our experiment values are considered to be reasonable.

3.2. Fluorescent characteristics

The BTOS phosphors indicate that divalent Ba^{2+} is replaced by trivalent Sm^{3+}, in which the charge imbalance will come into being. It will lead to a dramatically decreasing of emission spectra intensity [18]. Fig. 3 shows the spectra intensities of as-grown phosphors remarkably enhance with the increase of Na_2CO_3 doping concentration, and the spectra intensity of 3 wt% Na_2CO_3 doping BTOS phosphors is about 21.5(±0.3) times than that of pure BTOS phosphors. Here, a monovalent cation Na^+ in Na_2CO_3 acts as a charge compensator. It has been found that BTOS phosphors with tetragonal structure by doping with Na^+ ions show greatly enhanced reddish orange emission owing to the effective charge compensated behaviors [18], $2Ba^{2+} \rightarrow Sm^{3+} + Na^+$.

In Fig. 4, the excitation spectra of the reddish orange BTOS phosphors including 3 wt% Na_2CO_3 annealed at 1100 °C were exactly detected by the emission wavelength of about 595 nm. The excitation spectra consist of a series of sharp peaks originated from the *f–f* absorption of Sm^{3+} ion. In these excitation spectra, there is a characteristic excitation spectrum centered at 409 nm, which should be ascribed to $^6P_{3/2}$ (Γ_7) → $^6H_{5/2}$ (Γ_7) transition [11,4,10], suggesting that the excitation wavelength of as-grown phosphors matches well with the near-UV light LED chips. Besides, the other spectra centered at 382, 391, 422, 442, 465, 482 and 500 nm as well as their originations will be discussed in the next section.

As shown in Fig. 5, when the excitation wavelengths of 409 nm, as-grown phosphors produce the sharp and abundant emission peaks of Sm^{3+} in host crystals $BaTiO_3$ centered at 535, 561, 595, 637, 643, 647 and 701 nm. Obviously, among them, three main peaks centered at 561, 595 and 643 nm should be ascribed to $^4G_{5/2}$ (Γ_7) → $^6H_{5/2}$ (Γ_7), $^4G_{5/2}$ (Γ_7) → $^6H_{7/2}$(Γ_7) and $^4G_{5/2}$(Γ_7) → $^6H_{9/2}$(Γ_7) transitions of Sm^{3+} [10,11,4], respectively. More importantly, the fluorescence quenching of as-grown phosphors takes effect when so low 2% Sm^{3+}-doped concentration, which would effectively reduce the usage quantity of expensive rare earth elements and then dramatically decrease the cost of as-grown phosphors for white LEDs. In addition, in Fig. 6, the CIE

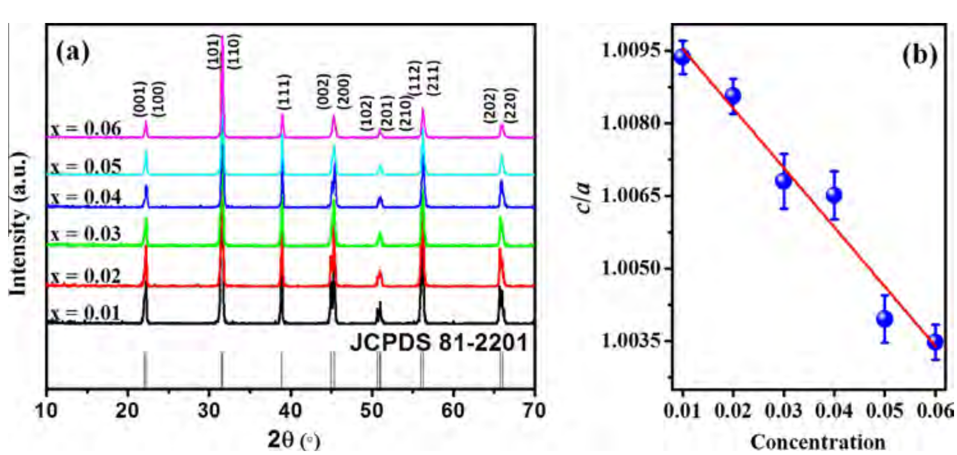

Fig. 1. The crystal structure of $Ba_{1-x}SiO_3$: Sm_x (x = 0.01–0.06) phosphors: (a) XRD patterns and (b) c/a ratio of various concentrations.

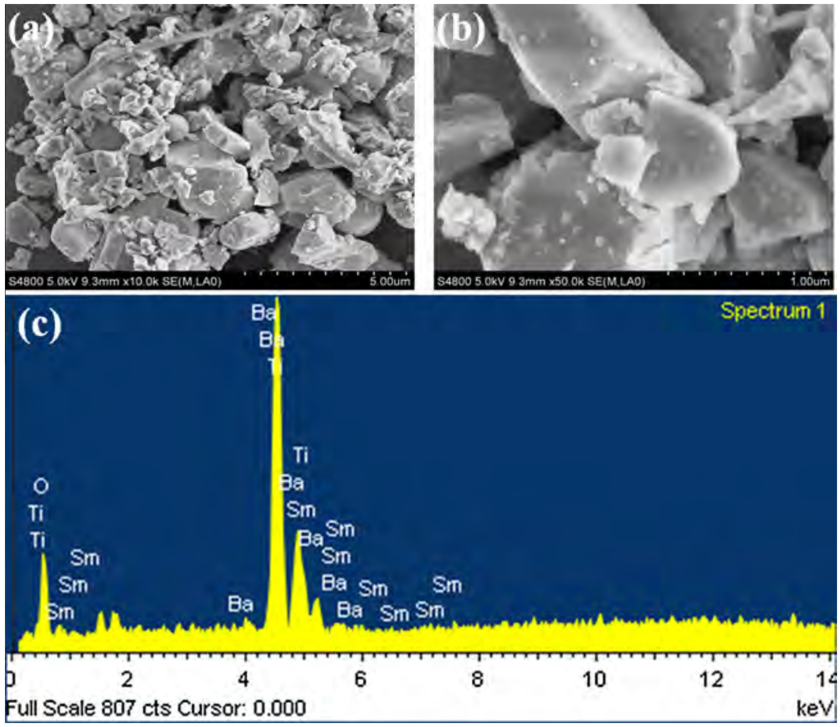

Fig. 2. The surface macroscopic images of $Ba_{0.98}SiO_3$: $Sm_{0.02}$ phosphors: (a) SEM, (b) enlarged SEM, and (c) EDS images.

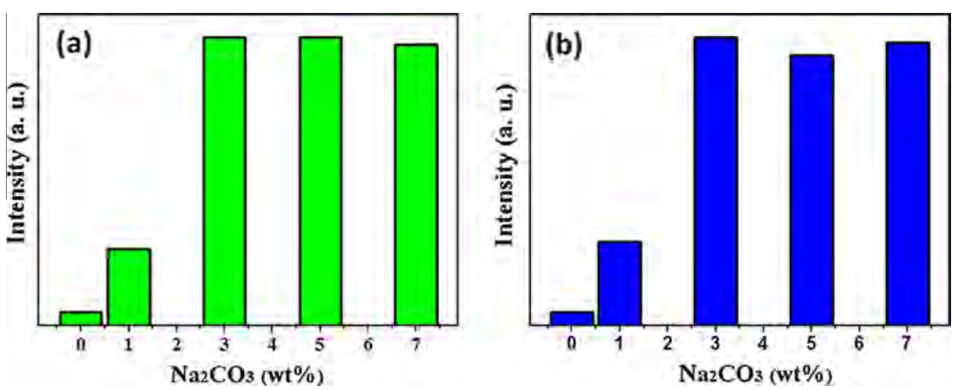

Fig. 3. Excitation (a) and emission (b) spectra intensities of BTOS phosphors with the various Na_2CO_3 doping concentrations.

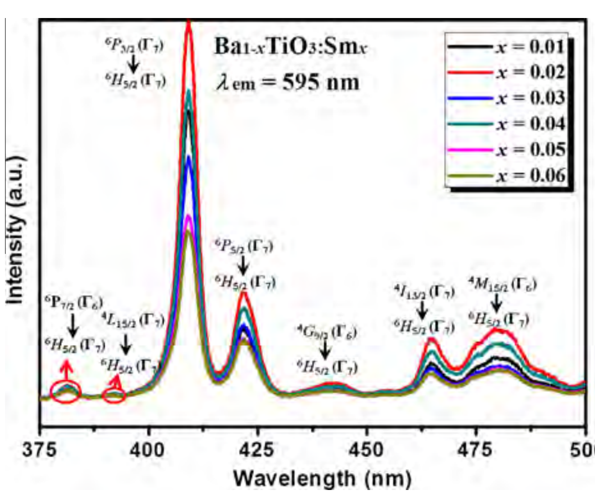

Fig. 4. Excitation spectra of $Ba_{1-x}SiO_3$: Sm_x (x = 0.01–0.06) phosphors with emission wavelength 595 nm.

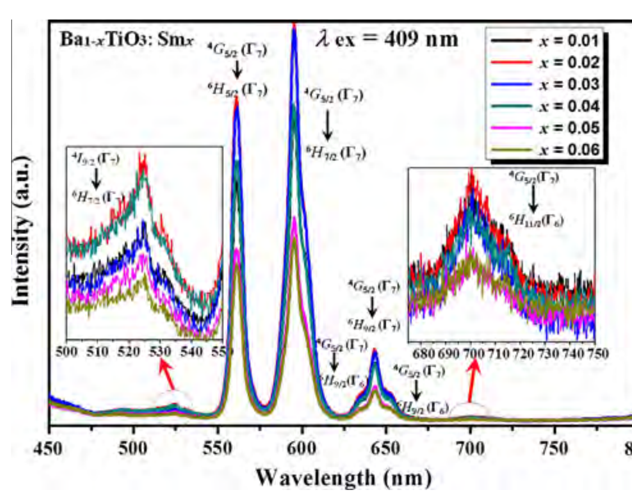

Fig. 5. The emission spectra of phosphors at $Ba_{1-x}SiO_3$: Sm_x (x = 0.01–0.06) phosphors with excitation wavelength 409 nm.

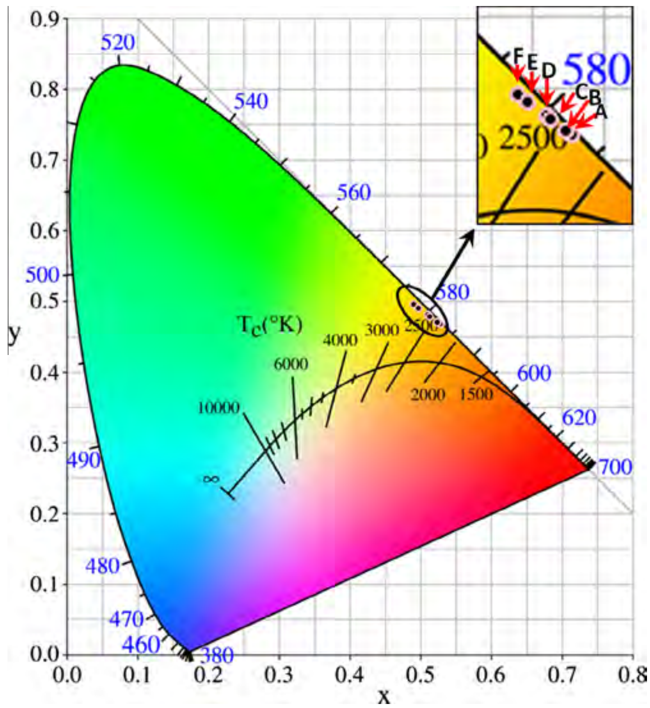

Fig. 6. CIE chromaticity coordinates of $Ba_{1-x}SiO_3$: Sm_x phosphors (x = 0.01 (A), 0.02 (B), 0.03 (C), 0.04 (D), 0.05 (E) and 0.06 (F)) with near UV-light 409 nm.

chromaticity coordinates gradually move from red to orange with an increase of Sm-doped concentration, suggesting Sm-doped concentration can effectively tune the CIE chromaticity coordinates of as-grown phosphors (see Fig. 7).

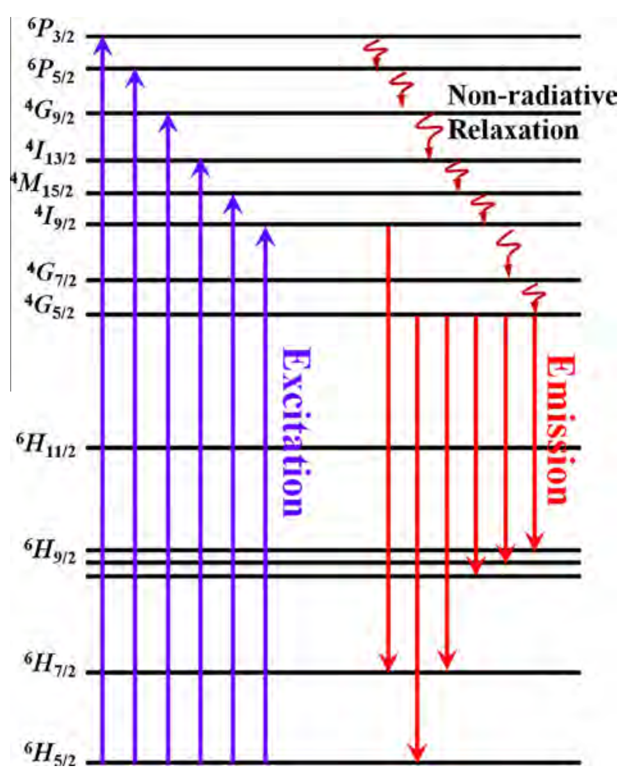

Fig. 7. The diagram of the luminescence mechanism of Sm^{3+} ion doped $BaTiO_3$ phosphors for white LEDs.

3.3. Crystal field analysis

From a theoretical point of view, the optical spectroscopy (or crystal field spectra) of rare earth ions in crystals can be explained by the widely used parametric modeling method [19]. In $BaTiO_3$ crystal, the effective Hamiltonian for the doped Sm^{3+} ion can be written concisely as

$$H = H_{FI} + H_{CF} \tag{1}$$

in which the free-ion Hamiltonian H_{FI} can be explicitly expressed as

$$H_{FI} = E_{avg} + \sum_{k=2,4,6} F^k \hat{f}_k + \zeta_{4f}\hat{A}_{SO} + \alpha\hat{L}^2 + \beta\hat{G}(G_2) + \gamma\hat{G}(R_7) + \sum_{i=2,3,4,6,7,8} T^i\hat{t}_i + \sum_{j=0,2,4} M^j\hat{m}_j + \sum_{k=2,4,6} P^k\hat{p}_k \tag{2}$$

The meaning of each term (including interaction operator and its coefficient) in Eq. (2) can be found in some pertinent reviews and monographs [19–23]. The concrete form of crystal field Hamiltonian H_{CF} in Eq. (1) is closely related to the local site symmetry around the central ion. For undoped $BaTiO_3$ crystal, both host ions Ba^{2+} and Ti^{4+} occupy the site with tetragonal C_{4v} symmetry. When a Sm^{3+} ion replaces the position of Ba^{2+} ion, the crystal field surrounding the Sm^{3+} ion should not be regarded as the same to the Ba^{2+} ion since the charge compensation and size mismatch between the two ions would probably cause local distortions on the host lattice after doping. Nevertheless, it is still reasonable to assume that a tetragonally-distorted crystal field could be formed around Sm^{3+} ion in $BaTiO_3$ crystal. Therefore, the crystal field interaction H_{CF} in Eq. (1) under tetragonal C_{4v} symmetry can be written, in the Wybourne notation [22], as [20]

$$H_{CF} = B_{20}C_{20} + B_{40}C_{40} + B_{44}(C_{44} + C_{4,-4}) + B_{60}C_{60} + B_{64}(C_{64} + C_{6,-4}) \tag{3}$$

where B_{kq} are crystal field parameters (CFPs) and C_{kq} are the Racah spheric tensor operators.

In general, the experimental optical spectra, i.e. transitions between different crystal field energy levels for $BaTiO_3$: Sm^{3+} crystal can be obtained by diagonalizing the complete 2002 × 2002 energy matrix of Hamiltonian H in Eq. (1) on the basis set of comprehensively adopted multiplets $^{2S+1}L_J$ [19,20] and each parameter characterizing the strength of interaction in Eqs. (2) and (3) is also determined by fitting procedures seeking the minimum of root mean square (RMS) deviation σ [20] between experimental and calculated optical spectra. Nevertheless, only sixteen intraconfigurational f–f transitions are observed by our experiments, which mean that the number of free variables (twenty free-ion parameters in Eq. (2) and five CFPs in Eq. (3)) is greater than that of experimental results in fitting calculations. This will cause the 'over-fit' problem [24] and obtain spurious empirical parameters. For this reason, in our calculations, we take the values of Sm^{3+} ion at cubic crystal field reported in [25], i.e., $E_{avg} \approx 47072\ \mathrm{cm}^{-1}$, the Coulomb repulsions $F^2 \approx 78016\ \mathrm{cm}^{-1}$, $F^4 \approx 56354\ \mathrm{cm}^{-1}$, $F^6 \approx 39737\ \mathrm{cm}^{-1}$, the two-body and three-body interaction parameters $\alpha \approx 21.3\ \mathrm{cm}^{-1}$, $\beta \approx -710\ \mathrm{cm}^{-1}$, $\gamma \approx 1699\ \mathrm{cm}^{-1}$, $T^2 \approx 246\ \mathrm{cm}^{-1}$, $T^3 \approx 25\ \mathrm{cm}^{-1}$, $T^4 \approx 18\ \mathrm{cm}^{-1}$, $T^6 \approx -158\ \mathrm{cm}^{-1}$, $T^7 \approx 253\ \mathrm{cm}^{-1}$, $T^8 \approx 379\ \mathrm{cm}^{-1}$, the Marvin integrals $M^0 \approx 2.48\ \mathrm{cm}^{-1}$, $M^2 \approx 0.56M^0 \approx 1.39\ \mathrm{cm}^{-1}$, $M^4 \approx 0.38M^0 \approx 0.94\ \mathrm{cm}^{-1}$, the parameters related to the electrostatic correlated magnetic interaction $P^2 \approx 359\ \mathrm{cm}^{-1}$, $P^4 \approx 0.75P^2 \approx 269\ \mathrm{cm}^{-1}$, $P^6 \approx 0.5P^2 \approx 180\ \mathrm{cm}^{-1}$ and the spin–orbit parameters $\zeta_{4f} \approx 1164\ \mathrm{cm}^{-1}$. Hence, only five CFPs (B_{kq}) are treated as adjustable parameters and their initio values for fitting can be estimated by superposition model [26] based on crystal structure of undoped $BaTiO_3$ and intrinsic CFPs of Sm^{3+} ion with oxygen ligands given in [27]. The best fitted CFPs with RMS σ equal to 30 cm^{-1} are obtained as (in cm^{-1}):

Table 1
The calculated and experimental energy levels (in cm^{-1}) of Sm^{3+} ion in $BaTiO_3$ crystals.

Multiplet	Irreps	Calc.	Expt.	ΔE
$^6H_{5/2}$	Γ_7	−18	0	18
	Γ_6	22		
	Γ_7	123		
$^6H_{7/2}$	Γ_6	894		
	Γ_7	997	1012	15
	Γ_7	1246		
	Γ_6	1387		
$^6H_{9/2}$	Γ_6	2082	2125	−43
	Γ_7	2234	2272	38
	Γ_6	2373	2377	4
	Γ_7	2444		
	Γ_6	2575		
$^6H_{11/2}$	Γ_7	3445		
	Γ_6	3531	3554	23
	Γ_6	3578		
	Γ_7	3695		
	Γ_6	3794		
	Γ_7	3863		
$^4G_{5/2}$	Γ_7	17,561		
	Γ_6	17,698		
	Γ_7	17,870	17,819	−51
$^4G_{7/2}$	Γ_6	19,708		
	Γ_7	19,815		
	Γ_6	19,882		
	Γ_7	19,947		
$^4I_{9/2}$	Γ_6	20,008	19,992	−16
	Γ_7	20,096	20,067	−29
	Γ_7	20,149		
	Γ_6	20,238		
	Γ_6	20,336		
$^4M_{15/2}$	Γ_7	20,519		
	Γ_7	20,580		
	Γ_7	20,670		
	Γ_6	20,690		
	Γ_7	20,730		
	Γ_6	20,742	20,764	22
	Γ_6	20,896		
	Γ_7	20,999		
$^4I_{13/2}$	Γ7	21,306		
	Γ6	21,377		
	Γ7	21,391		
	Γ6	21,442		
	Γ7	21,520	21,515	−5
	Γ7	21,533		
	Γ6	21,537		
$^4G_{9/2}$	Γ7	22,621		
	Γ6	22,645	22,645	0
	Γ7	22,700		
	Γ6	22,838		
	Γ6	22,891		
$^6P_{5/2}$	Γ7	23,706	23,708	2
	Γ6	23,723		
	Γ7	23,754		
$^6P_{3/2}$	Γ7	24,472	24,426	−46
	Γ6	24,481		
$^4G_{11/2}+{}^4L_{15/2}$	Γ6	25,351		
	Γ7	25,438		
	Γ6	25,440		
	Γ7	25,483		
	Γ7	25,506		
	Γ6	25,519		
	Γ7	25,557	25,549	−8
	Γ6	25,593		
	Γ6	25,606		
	Γ6	25,657		
	Γ7	25,702		
	Γ7	25,726		
	Γ6	25,770		
	Γ7	25,806		
$^6P_{7/2}$	Γ6	26,220	26,192	−28
	Γ7	26,252		
	Γ7	26,261		
	Γ6	26,400		

$$B_{20} \approx 117(39),\ B_{40} \approx 272(32),\ B_{44} \approx 1167(66),\ B_{60} \approx 165(95),\ B_{64} \approx -2114(57) \quad (4)$$

The calculated optical spectra and their labels, i.e. irreducible representations (IRREPs) are listed and compared with the experimental ones in Table 1 and Fig. 6. Please note that only the multiplets to which the experimental optical spectra are assigned are given in the listing.

From Table 1 and Fig. 6, it can be found that the calculated optical spectra of $BaTiO_3$: Sm^{3+} phosphors are in reasonable agreement with the experimental results, showing that the crystal field modeling is effective for explaining the excitation and fluorescence spectra of the studied phosphors. However, the disparities between calculated and experimental values in Table 1 may be ascribed to two reasons: (i) The light intensity of the xenon lamp in the used spectrophotometer makes it difficult to test the fine fluorescence spectra of phosphors. So, the tested spectra are often broad and the maximum of the fluorescent peak usually acts as the final result. (ii) The twenty free-ion parameters which dominantly determine the optical band positions of rare earth ions in crystals are not obtained by fitting procedures but kept at some fixed values in order to solve the 'over-fit' problem. This, however, will cause some calculated errors for optical spectra in Table 1 since these parameters in Eq. (2) are slightly different from crystal to crystal [20,21] due to the different covalence effect of crystals.

4. Conclusions

To sum up, we reported the reddish orange BTOS phosphors for white LEDs by the simple solid state reaction method. The near ultraviolet light (409 nm) can effectively excite the reddish orange as-grown phosphors to produce exceptionally powerful reddish orange light consisted of three peaks centered at 561 nm, 595 nm and 637 nm. It obtained that Na_2CO_3 as a charge compensator could dramatically enhance the emission intensity of BTOS phosphors and its best doping concentration should be 3 wt%. More importantly, the complete 2002×2002 energy matrix of Sm^{3+} ion at the tetragonal (C_{4v}) Ba^{2+} site of perovskite $BaTiO_3$ crystal was successfully found to accurately and quantitatively identify the corresponding spectra by a diagonalization (of energy matrix) method for the first time, suggesting a novel method to make clear the luminescent mechanism of Sm^{3+}-doped phosphors for w-LEDs. Also, it evidently demonstrates the feasibility of the complete diagonalization method to investigate the other rare earth elements doping phosphors for w-LEDs, and then provides a new train of thought and tactics for the development and utilization of novel fluorescent materials.

Acknowledgements

This work is supported by the National Natural Science Foundation of China (Nos. 51202023 and 11028409), the Scientific and Technological projects for distinguished Young Scholars of Sichuan Province (No. 2015JQ0013), the Fundamental Research Funds for the Central Universities of China (A0920502051408-10 and ZYGX2009Z0001). The authors are also grateful to Prof. Yau Yuen Yeung of the Hong Kong Institute of Education for providing us with the ''*f*-shell Crystal Field Analysis Package''.

References

[1] W.Z. Lv, Y.C. Jia, Q. Zhao, M.M. Jiao, B.Q. Shao, W. Lu, H.P. You, Adv. Opt. Mater. 2 (2014) 183–188.
[2] T.M. Tolhurst, T.D. Boyko, P. Pust, N.W. Johnson, W. Schnick, A. Moewes, Adv. Opt. Mater. (2015), http://dx.doi.org/10.1002/adom.201400558.
[3] P. Pust, V. Weiler, C. Hecht, A. Tücks, A.S. Wochnik, A.K. Henß, D. Wiechert, C. Scheu, P.J. Schmidt, W. Schick, Nat. Mater. 13 (2014) 891–896.
[4] V.R. Bandi, B.K. Grandhe, M. Jayasimadri, K. Jang, H.S. Lee, S.S. Yi, J.H. Jeong, J. Cryst. Growth 326 (2011) 120–123.
[5] H.A. Höppe, Angew. Chem. Int. Ed. 48 (2009) 3572–3582.
[6] W.Q. Yang, H.G. Liu, G.K. Liu, Y. Lin, M. Gao, X.Y. Zhao, W.C. Zheng, Y. Chen, J. Xu, L.Z. Li, Acta Mater. 60 (2012) 5399–5407.
[7] W.Q. Yang, H.G. Liu, M. Gao, Y. Bai, J.T. Zhao, X.D. Xu, B. Wu, W.C. Zheng, G.K. Liu, Y. Lin, Acta Mater. 61 (2013) 5096–5104.
[8] B. Wu, W.Q. Yang, H.G. Liu, Li Huang, B.W. Zhao, C. Wang, G.L. Xu, Y. Lin, Spectr. Acta Part A: Mol. Biomol. Spectr. 123 (2014) 12–17.
[9] V.R. Bandi, Y.T. Nien, T.H. Lu, I.G. Chen, J. Am. Ceram. Soc. 92 (2009) 2953–2956.
[10] M. Ganguly, S.K. Rout, W.S. Woo, C.W. Ahn, I.W. Kim, Physica B 411 (2013) 26–34.
[11] D.P. Dutta, A. Ballal, J. Nuwad, A.K. Tyagi, J. Lumin. 148 (2014) 230–237.
[12] P. Zhu, Q. Zheng, R. Sun, W.J. Zhang, J.H. Gao, C.P. Wong, J. Alloys Comp. 614 (2014) 289–296.
[13] D. Xu, W.L. Li, L.D. Wang, W. Wang, W.P. Cao, W.D. Fei, Acta Mater. 79 (2014) 84–92.
[14] A.R. Damodaran, E. Breckenfeld, Z.H. Chen, S. Lee, L.W. Martin, Adv. Mater. 26 (2014) 6341–6347.
[15] S. Makishima, K. Hasegawa, S. Shionoya, J. Phys. Chem. Solids 23 (1962) 749–757.
[16] S. Makishima, H. Yamamoto, T. Tomotsu, S. Shionoya, J. Phys. Soc. Jpn. 20 (1965) 2147–2151.
[17] V.M. Longo, M.G.S. Costa, A.Z. Simões, I.L.V. Rosa, C.O.P. Santos, J. Andrés, E. Longoa, J.A. Varelaa, Phys. Chem. Chem. Phys. 12 (2010) 7566–7579.
[18] Z.G. Xia, D.M. Chen, J. Am. Ceram. Soc. 93 (2010) 1397–1401.
[19] G.K. Liu, in: G.K. Liu, B. Jacquier (Eds.), Spectroscopic Properties of Rare Earths in Optical Materials, Springer, Berlin, 2005 (Chapter 1).
[20] C. Görller-Walrand, K. Binnemans, in: K.A. Gschneidner Jr., L. Eyring (Eds.), Handbook on the Physics and Chemistry of Rare Earths, vol. 23, Elsevier, Amsterdam, 1996.
[21] S. Hüfner, Optical Spectra of Transparent Rare Earth Compounds, Academic Press, New York, 1978.
[22] B.G. Wybourne, Spectroscopic Properties of Rare Earths, Wiley, New York, 1965.
[23] R.D. Cowan, The Theory of Atomic Structure and Spectra, University of California Press, Berkeley, 1981.
[24] L.H. Xie, Y.Y. Yeung, Appl. Magn. Reson. 44 (2013) 917–925.
[25] C.K. Duan, P.A. Tanner, J. Phys. Chem. A 114 (2010) 6055–6062.
[26] D.J. Newman, B. Ng, Rep. Prog. Phys. 52 (1989) 699–763.
[27] W.Q. Yang, W.C. Zheng, P. Su, H.G. Liu, Z. Naturforsch. A 66 (2011) 139–142.